Book of Tutorials and Abstracts

European Microbeam Analysis Society

EMAS 2025

18th

EUROPEAN WORKSHOP

on

MODERN DEVELOPMENTS AND APPLICATIONS IN MICROBEAM ANALYSIS

11 to 15 May 2025
at the
TecnoCampus
Mataró (Barcelona), Spain

Organized in collaboration with the
Universitat de Barcelona, Spain

EMAS
European Microbeam Analysis Society eV
www.microbeamanalysis.eu/

This volume is published by:
European Microbeam Analysis Society eV (EMAS)
EMAS Secretariat
c/o Eidgenössische Technische Hochschule, Institut für Geochemie und Petrologie
Clausiusstrasse 25
8092 Zürich
Switzerland

ISBN 978 90 8227 6985
NUR code: 972 – Materials Science

POSSIBILITIES AND LIMITATIONS OF Li-DETECTION AND QUANTIFICATION IN ELECTRON BEAM ANALYSIS

Ute Golla-Schindler and G. Schneider
Aalen University, Materials Research Institute (IMFAA)
Beethovenstrasse 1, 73430 Aalen, Germany
e-mail: ute.golla-schindler@hs-aalen.de

Dr. rer. nat. Ute Golla-Schindler was born in 1968, married 2000, and has one son (born 2008). She studied in Münster (Germany) where she obtained her Diploma and PhD in electron microscopy. Her MSc work dealt with: "*Measurement of transmission and backscattering in low-voltage scanning electron microscopy*" (supervisor Prof. L. Reimer), while her PhD was about: "*Investigation of resolution and detection limits in element distribution images (TEM)*" (Supervisor Prof. H. Kohl). In 1997 she became Lecturer and research scientist in the Institute of Mineralogy at the University Münster. In 2001 she became application specialist scanning electron microscopy for Carl Zeiss NTS GmbH in Oberkochen. In 2002 she became responsible for the TEMs of the electron microscopy laboratory (ICEM Interdisciplinary Centre for Electron Microscopy) of the University of Münster, where she worked on exsolution phenomena and magnetic properties in minerals and the toxicology of nanoparticles. In 2010 she became senior scientist in the electron microscopy group of material science at the University of Ulm working on radiation damage effects in electron microscopy and group leader for battery materials. Since April 2016 she is senior scientist in the material research institute at the University of Aalen, working on energy related materials.

1. INTRODUCTION

Energy storage is one of the major challenges on the road to environmental protection. The most commonly used batteries today and in the near future are Li-ion based systems. Therefore, it is very important to develop workflows and methods that can reliably detect Li and ideally also quantify its content.

In general, the detection and especially the quantification of Li is not straightforward. For energy dispersive X-ray spectroscopy (EDS), the cross-section for the generation of Li-Kα X-rays is very small. The competing process for X-ray production is the emission of an Auger electron, which becomes more likely with decreasing atomic number. In the unoccupied state Li has three electrons, two in the K shell (1s energy state) and one in the L1 (2s energy state). The electric dipole transition provides the most intense X-ray lines, and for the transition from the Li-L1 to the K-shell the electric dipole selection rule $\Delta l = \pm 1$ is not fulfilled. Additionally, when Li is in a covalently or ionically bonded state, there is no electron left from a higher shell to fill the hole in the K-shell, forming a Li-Kα X-ray.

Further possibilities to detect Li are energy loss spectroscopy (EELS), mass spectrometry (MS), inductively coupled plasma optical emission spectroscopy (ICP-OES), X-ray photoelectron spectroscopy (XPS), and laser induced breakdown spectroscopy (LIBS). These methods can overcome the restriction of X-ray analysis. However, they have other limitations such as lower spatial resolution (XPS), high time expenditure, more sophisticated sample preparation, that may not be free of artefacts (EELS), lower spatial resolution and higher beam currents, which increase the possibility of radiation damage (MS, SXES), destructive analysis methods that also provide a significantly lower spatial resolution (ICP-OES, LIBS).

EDS is the method of choice when high spatial resolution and the analysis of µm-scale sample areas are required. If you also want to explore the field of quantitative analysis with high spatial resolution and the lowest possible detection limits, one point that becomes extremely important is the awareness of sample changes during or by the analytical investigation. In scanning electron microscopy (SEM), for example, radiation damage caused by the interaction of the electron beam with the sample, contamination (the growth of carbon on the surface of the sample from cracked hydrocarbon compounds) and insufficient electrical conductivity, which manifests itself as charging, can significantly affect the result.

The main topic of the paper is the new opportunities and challenges of low energy X-ray detection using EDS in the field of Li-ion battery analysis. The windowless Oxford Extreme EDS detector overcomes the bottleneck of Li detection and opens new perspectives in this field [1]. During the development process, windowless detection was combined with improved electrical amplification, leading to a further improvement in detection capabilities. This detector allows EDS investigations with lower accelerating voltages and beam currents. This can have a significant impact on the reduction of examination artefacts, or even make examinations

possible at all. Studies with this detector have already shown that detection of Li in Li metal and Li compounds is possible in samples without topography [1-5]. In the following, we will look at the possibilities for investigations, from Li detection to quantification, in the context of the application on real issues related to Li-ion batteries.

2. CHARGING, CONTAMINATION, RADIATION DAMAGE

If the electrical conductivity of the sample is insufficient "charging" can occur, when the primary energy of the incident electrons is above the E2 point [6]. The amount of incoming and outgoing electrons is equal at the E2 point. For higher landing energies than the E2 point the absorbed probe current exceeds the amount of generated backscattered and secondary electrons, the left-over electrons charge up the sample negatively. This continuously changes the landing energy of the primary electrons and thus the cross-section for the element-specific X-ray generation. This error cannot be corrected by post-processing. To check this, the Duane-Hunt limit [7], where the continuum (Bremsstrahlung) of the X-ray flux goes to zero, can be compared with the expected landing energy of the incident electrons. As the sample is charged, the value of the Duane-Hunt limit decreases [7-9].

There are two approaches to reduce or avoid charging. The classical approach is to coat the sample with a conductive material. This coating then also contributes to the EDS signal and cannot be easily separated. The second approach is to reduce the accelerating voltage. With decreasing accelerating voltage, the effective cross-sections for the elastic and inelastic interaction increase and thus the number of secondary and backscattered electrons generated. If the primary energy of the incident electrons approaches the E2 point, the number of electrons remaining in the sample decreases. This reduces or avoid charging effects.

The next topic is carbon contamination, which is the electron beam induced decomposition of carbon-rich compounds (hydrocarbons) and their subsequent deposition on the sample surface [6, 10-12]. They originate from the sample itself or from the vacuum (residual gas molecules). This effect becomes increasingly critical with decreasing acceleration voltage, as the interaction volume decreases with decreasing acceleration voltage. Consequently, the contribution of the contamination layer to the EDS signal increases.

An additionally critical factor is beam damage, especially for the detection of light elements. Here, the benefit for low voltage application strongly depends on the main damage mechanism. If the accelerating voltage decreases, the knock-on damage is reduced, but the beam damage caused by heating and ionisation is possibly enhanced due to the increasing cross-sections for inelastic and elastic scattering. Lowering the beam current, beam current density will reduce all beam damage effects [13-17]. Figure 1 shows scanning electron micrographs of Al (Figs. 1a and 1b), Si (Figs. 1c and 1d), and Li metal (Figs. 1e and 1f) obtained with a Zeiss Crossbeam 540 SEM. Figures 1a, 1c and 1e were recorded with the chamber secondary electron (SE) detector

(ETD, Zeiss SESI); Figs. 1b, 1d and1f with the Inlens detector with a landing energy of 3.5 keV, a current of 300 pA at a magnification of 15,000× for Figs. 1a and 1c (calibrated to polaroid), and a magnification of 2,000× for Figs. 1e and 1f. All images were taken after EDS point and area analysis and the right and left images were recorded simultaneously in dual imaging mode.

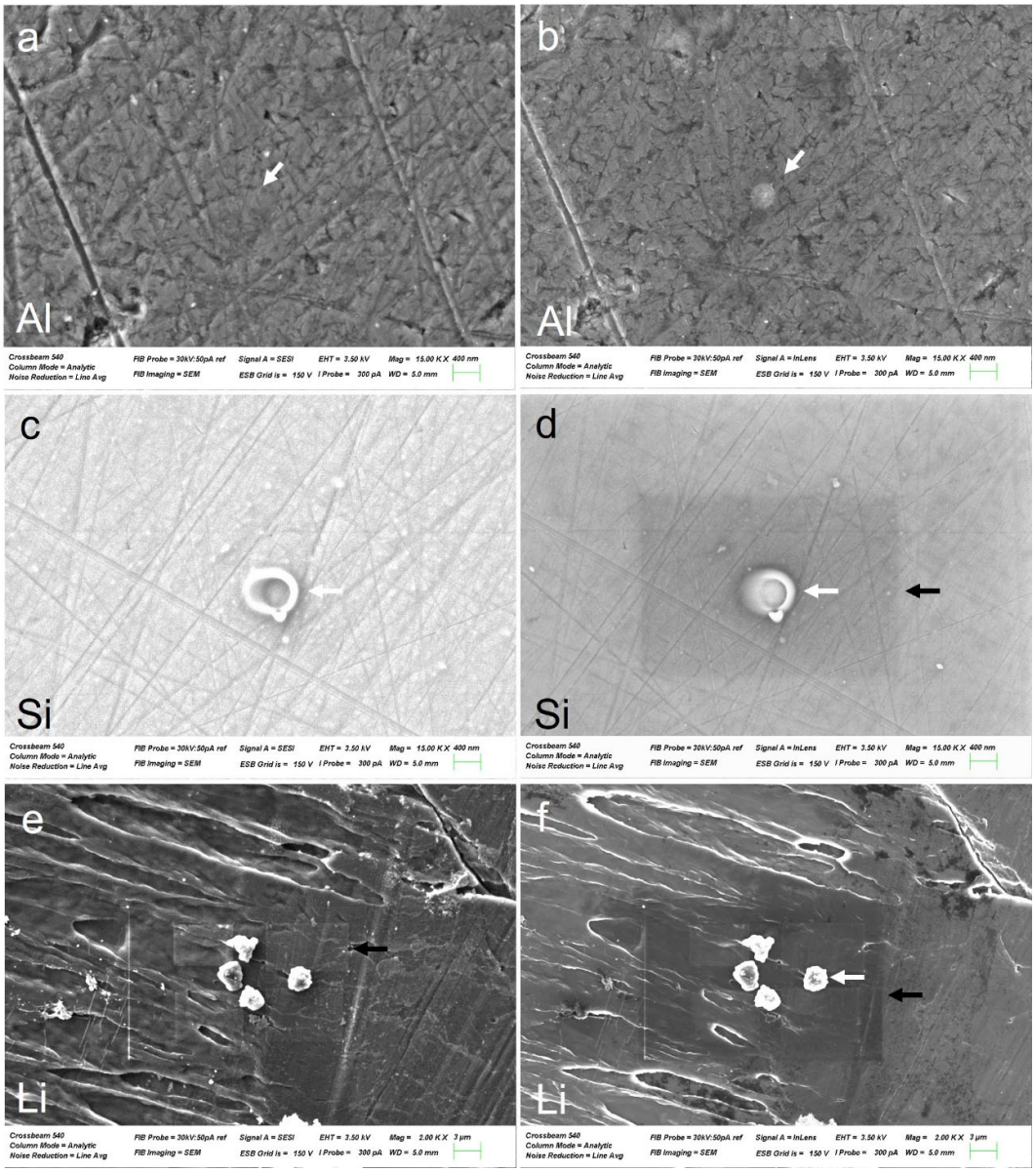

Figure 1. Scanning electron micrographs of Al, Si and Li after EDS analysis; a, c and e) with the chamber SE detector, and b, d and f) with the Inlens detector.

Comparing the Al image in Figs. 1a with 1b, the sample change due to radiation damage at the location of the EDS point analysis is only visible in the image obtained with the Inlens detector (white arrow). In the case of Si, sample changes occurred in both the point and area analysis. This time the influence of the radiation damage from the point analysis is observable in both the SE chamber image and the Inlens image (white arrows). The contamination of the sample surface caused by the area scan is only visible in the Inles image (black arrow).

The images of Li after the EDS analyses show dramatic changes due to both radiation damage from the spot analysis (white arrows) and contamination. The classical material contrast in the Inlens image is superimposed by a potential contrast. This leads to a darker contrast for the carbon contamination of the large area scan (dark arrow) than the Li surface (Fig. 1f) of the Inlens detector. The image with the chamber SE detector (Fig. 1e) shows the correct material contrast, with the contamination of the large field examination barely visible. Only with increasing layer thicknesses, analysing smaller fields, does the carbon contamination appear with a bright material contrast in Fig. 1f.

Many investigations have been carried out to understand and avoid contamination. The transition between the deposition of contamination layers and radiation damage and the subsequent possible removal of material (surface etching) is fluid, depending on the investigation parameters. Temperature and beam currents play a crucial role. It is helpful to bake the sample if possible, to use plasma cleaning, beam showering (large area irradiation of the sample prior to examination) and to store the sample in a hydrocarbon-free vacuum as possible [6, 10-12]. It is important to realise that even if no sample changes are visible in the SEM image, significant sample changes may still be present. It is essential to choose the right detector and microscope settings to make these sample changes visible.

3. Li DETECTION, QUALITATIVE ANALYSIS

3.1. Li metal

In order to apply the possibilities of Li detection and quantification to the analysis of Li-ion batteries, the first step was to carry out investigations on Li metal. This involved testing different storage conditions, different sample transfers, and the ability to remove reaction layers using focussed ion beam (FIB). The spectra were recorded with a landing energy of 3.5 keV and a current of 500 pA.

Figure 2a shows the spectra of Li metal transferred from the glove box in a single stub holder container and installed in the air lock with brief (a few seconds) contact with air (black spectrum labelled argon/air). In the case of the spectrum shown in red, the Li metal stored in the glove box was transferred to the SEM using the new Zeiss single shuttle holder without air contact (labelled shuttle). The airlock was flushed with argon in advance to avoid contact with nitrogen.

The first pleasing result, Li can be clearly detected in both spectra. But both spectra show peaks of other elements, which means that in both cases the Li is already covered with a passivation layer. But these passivation layers are different. The sample with the shuttle transfer shows a significantly higher Li peak than in the spectrum of the argon/air sample. Furthermore, in the shuttle spectrum, the Li peak is the largest peak compared to the other detected elements. It can be seen that the sample taken with the shuttle from the glove box is also covered with a native passivation layer NPL [5]. However, it shows a significantly lower oxygen content and no nitrogen compared to the sample with the short contact with air. This native passivation layer on metallic Li and Li compounds has been intensively studied and characterised [5]. It was found that this layer consists of two sub-layers. Firstly, a Li_2CO_3 layer, which can for example be formed with the carbon atoms of hydrocarbons in the vacuum of the SEM, with a layer thickness of about 25 nm, and a second inner Li_2O layer, which was about 40 nm for metallic Li and about 100 nm for Li compounds. Calculating the electron range R at a landing energy of 3.5 keV using Monte Carlo simulations [18], one obtains R ~ 830 nm for Li, R ~ 520 nm for Li_2O, and R ~ 360 nm for Li_2CO_3. Calculations have been carried out using both the Rutherford and Mott cross-sections and both give approximately the same results. The information depth is approximately R/3. This means that with a conventional NPL layer, a portion of the metallic Li is still detected.

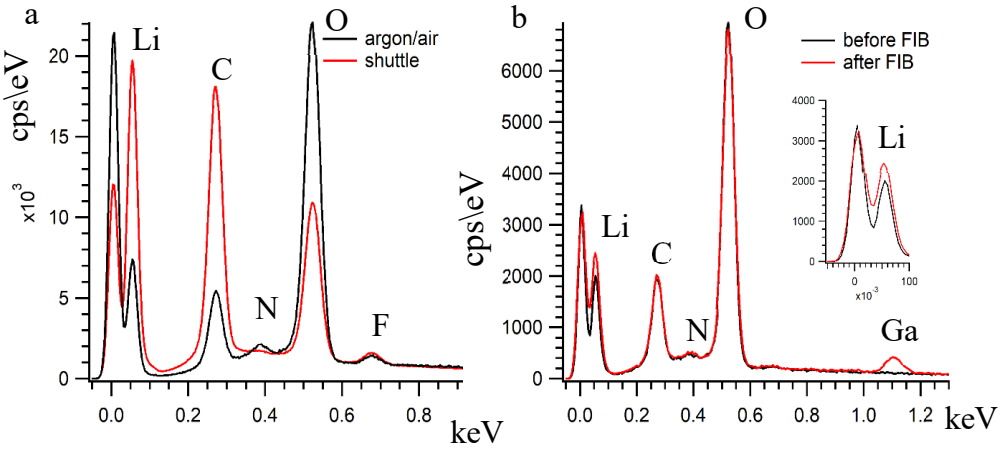

Figure 2. EDS spectra of a) Li metal comparing the effect of sample transfer, and b) before and after FIB material removal.

One idea was to clean the Li surface in the SEM by ablation with Ga^+-ions using a focussed ion beam (FIB). The surface was scanned for 2 minutes with a current of 50 pA. After this, Fig. 2b red spectrum (after FIB), shows an increase in the Li signal compared to the black spectrum (before FIB). Unfortunately, the incorporation of Ga is also clearly visible. After this initial examination, the sample with the shuttle transfer was returned into the single shuttle transfer and stored in the laboratory for eight days. It was then returned back into the microscope and

examined with a landing energy of 3.5 keV, a current of 300 pA and a magnification of 5,000× (calibrated to polaroid image size) and the images were recorded with the Inlens SE detector. Many reaction products were found on the surface, covering it to varying degrees (Fig. 3). Some areas are completely covered with a grown layer (Fig. 3a); these merge into areas that are partially covered with a crumbly layer, partly arranged in a thread-like manner (Figs. 3b and 3c). These are followed by areas that are still uncovered without the crumbly coating (Fig. 3d). All images are taken after the EDS examination.

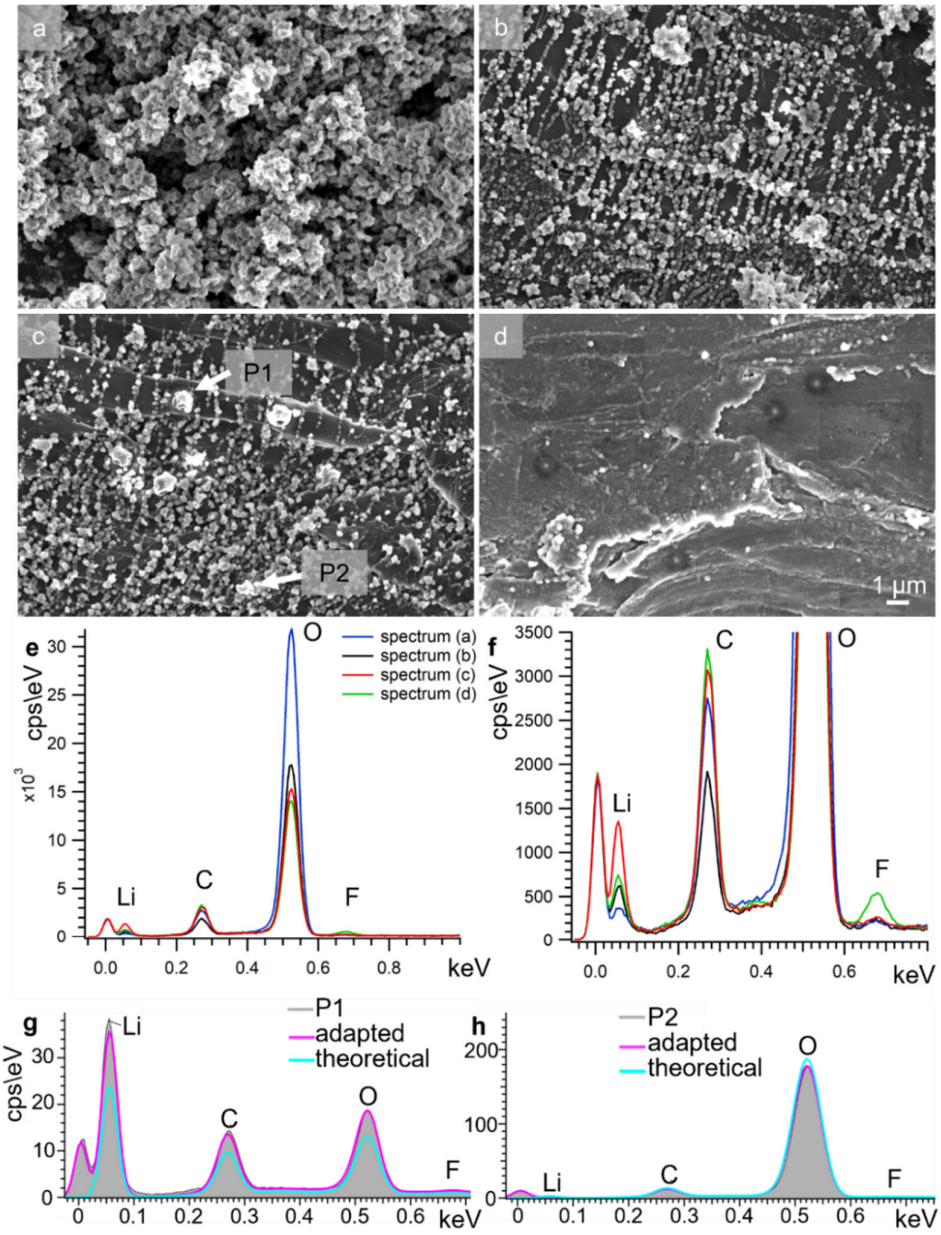

Figure 3. a to d) SEM images of a lithium metal sample after 8 days storage in a shuttle system, e and f) Correlated EDS spectra of the images, and g and h) correlated point EDS spectra, positions marked in image c).

The correlated spectra recorded over the entire image area are shown in Figs. 3e and 3f (enlarged section of Fig. 3e). The most striking features are the high oxygen content of spectrum a) of Fig. 3a, the high Li-content of spectrum c) of Fig. 3c, and the high F-content of spectrum d) of Fig. 3d. These results can be interpreted as the formation of oxygen-rich Li-compounds as the crumbly coating (Fig. 3a) and the original fluorine-rich passivation layer directly on the metallic Li (Fig. 3d).

EDS analysis can be used not only for the detection and qualitative estimation of elemental contents. It also allows the quantitative determination of elemental contents by means of standard-based or standard-free *k*-factors [8, 9, 19]. It is important to be aware of the sources of error and to avoid or reduce them as far as possible. Figures 3g and 3h show point spectra recorded in the image area shown as P1 and P2 in Fig. 3c. One is at a position without the crumbly coating and one is at a position with the crumbly coating. The position of the spectra in the image can be easily visualised after recorded based on the radiation damage that has occurred. Position P1 shows much more pronounced radiation damage and a very high Li-content in the spectrum, without fluorine. If an adapted spectrum (pink line) is calculated with the EDS Software (after the determination of the elements found), it still agrees well with the measurement. However, the theoretically calculated spectrum (blue line) shows significant deviations. The spectrum P2 on the crumbly coating shows less radiation damage, lower lithium and higher oxygen content and a very good agreement with both the adaptive (pink line) and the theoretically calculated spectrum (blue line). If a non-normalised quantitative determination of the elemental contents is carried out for both spectra, the deviation of the total content (which should be 100 %) is over 50 % for the spectrum at P1 and in a good agreement for the spectrum at P2. Calculating the atomic percentages for Li (65 %) and O (31 %) in P2 gives a ratio of 2:1 and Li_2O as the likely compound.

3.2. Li compounds, Li-ion batteries

In the next step, lithium-ion batteries with a chemistry of $LiFePO_4$ / graphite and $LiNiMnCoO_2$ / graphite+SiO_x are analysed. This involves the examination of unused and used batteries.

Figures 4a and 4b show SEM images of an aged Li-ion battery anode with $LiFePO_4$/graphite chemistry. The use of the battery has caused different kinds of deposits on the surface. Point analyses were recorded on these deposits at points marked P1, P2 in Fig. 4a and P3, P4 in Fig. 4b. These spectra are shown in Fig. 4c for point analyses P1 (grey), P2 (red). Figure 4d shows an enlarged section of the Li peak area. The spectra of the point analyses for P3 (grey), P4 (red) are shown in Fig. 4e and a sectional enlargement of the Li peak area in Fig. 4f. In both cases deliver the grey spectra in comparison with the red once clear differences in the Li edge region. It is important to check whether there are other elements present in the spectrum that also have transitions in this low-energy range. Possible candidates are Si-Lα (92 eV), in which

case the Kα 1.74 eV peak must also be present, or Al-Lα (72 eV), in which case the Kα 1.49 eV peak must also be present, or Fe M transitions, in which case the correlated Fe-Lα (704 eV) peak must be present. Since neither Al, Si nor Fe were detected in the entire spectrum, this peak can be reliably assigned to Li. Then it follows that, the darker area on the deposits in Fig. 4a and the spherical precipitate in Fig. 4b are Li-containing phases.

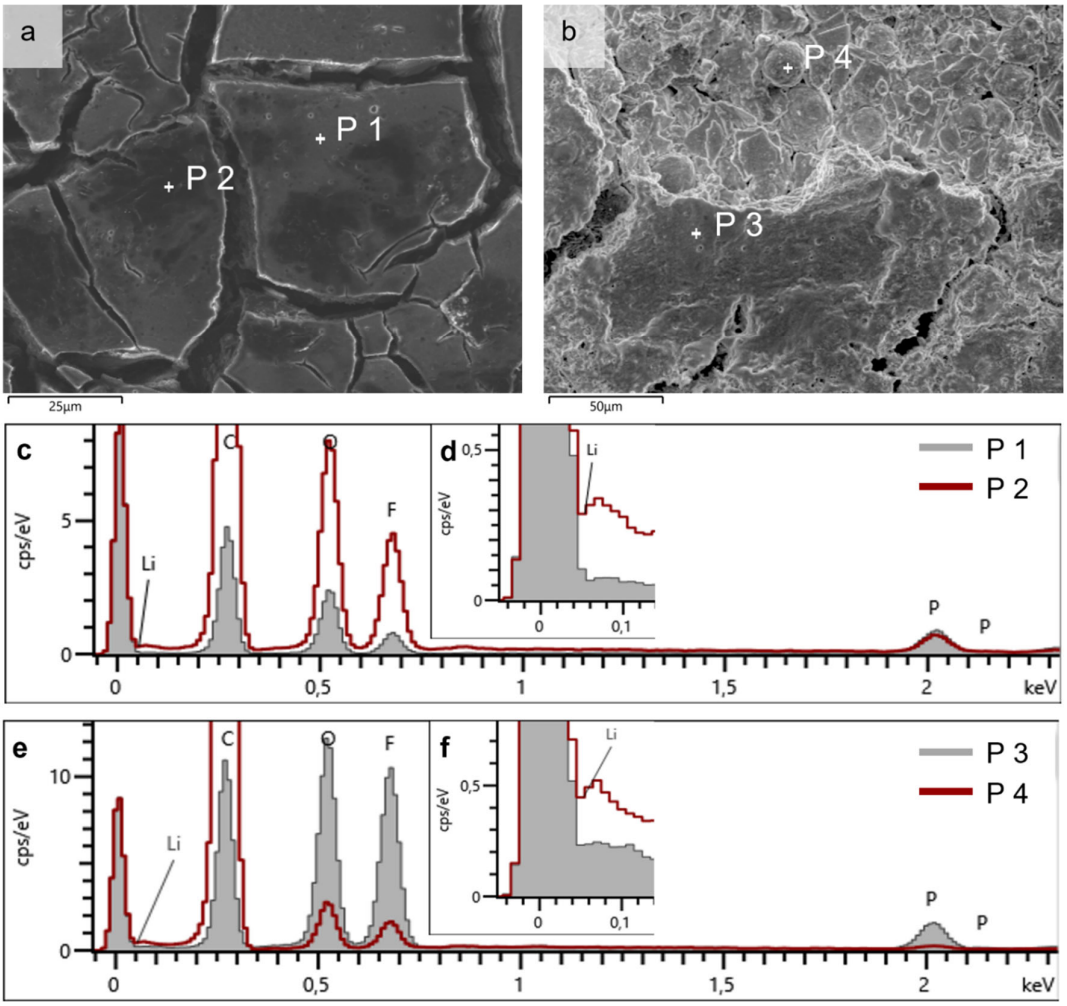

Figure 4. Analysis of an aged Li-ion battery with $LiFePO_4$ / graphite chemistry. a and b) SEM images of the anode surface, c and d) EDS spectra taken at positions P1 and P2 marked in a), and e and f), EDS spectra taken at positions P3 and P4 marked in b).

The next example shows the examination of an anode surface of a $LiNiMnCoO_2$ / graphite+SiO_x of an unused battery (LG18650 HG2). Figure 5a shows the SEM image and Figs. 5b to 5f the corresponding element distribution images of the elements: Fig. 5b – C-Kα, Fig. 5c – Si-Kα, Fig. 5d – O-Kα, Fig. 5e – F-Kα, and Fig. 5f – Al-Kα. Various phases can be seen: the majority are the graphite particles (Fig. 5b). Then there are smaller Si-rich particles that also have a high

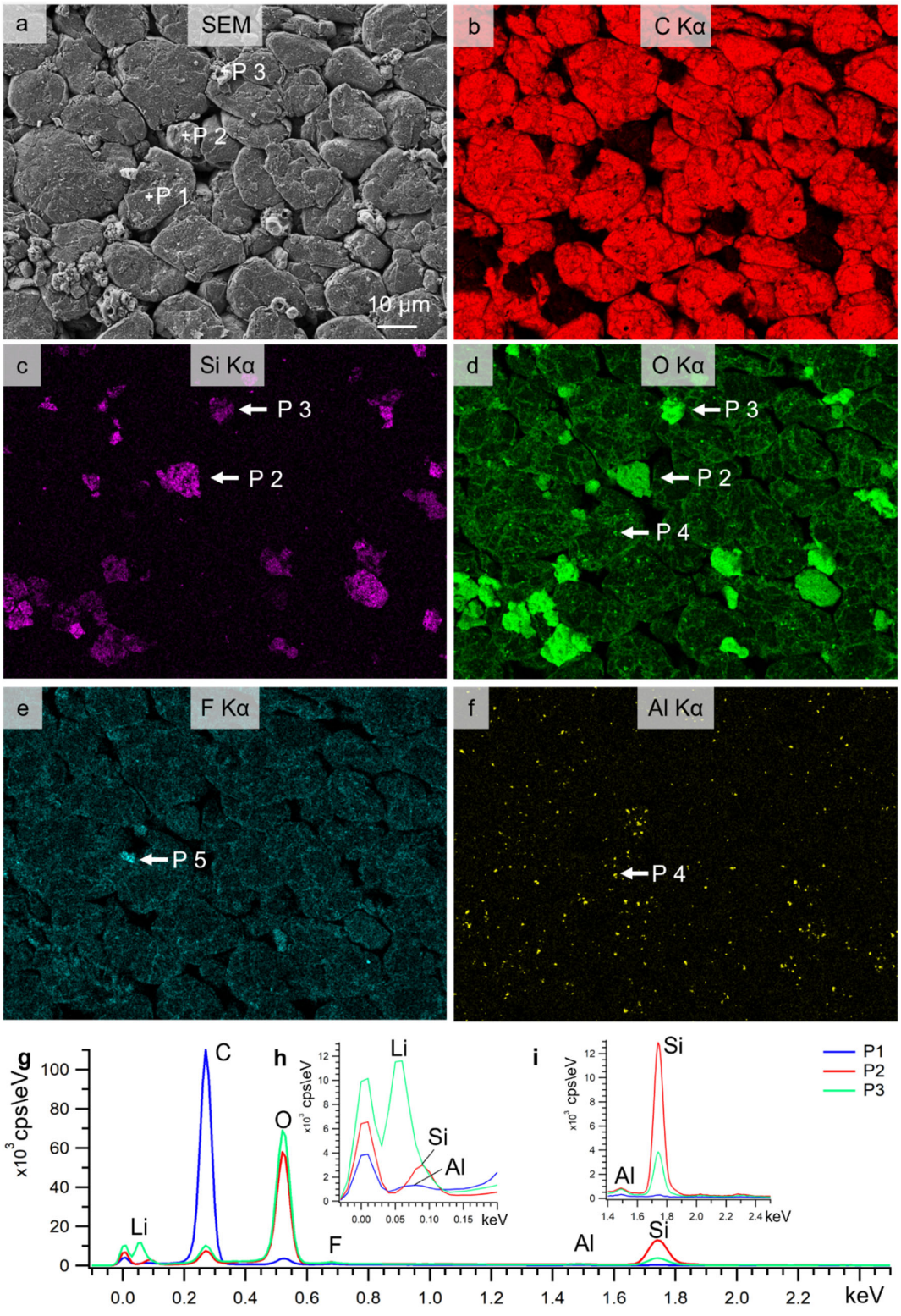

Figure 5. Examination of an anode surface of a lithium-ion battery using SEM and EDS. a) Image with the SE inlens detector; b to f) Element distribution images of: b) carbon, c) silicon, d) oxygen, e) fluorine, and f) aluminium.

oxygen content (Figs. 5c and 5d). There are two categories of those particles: particles with a lighter Si-signal and darker oxygen signal (marked as P2 in Figs. 5c and 5d) and particles with a darker Si-signal and a lighter oxygen signal (marked as P3 in Figs. 5c and 5d). Fluorine is found as a deposit on the graphite and there are also some small particles with a high F-content (marked as P5 in Fig. 5e), possibly residues of the electrolyte's conducting salt $LiPF_6$. Then there are small Al crumbs distributed on the anode surface that also contain oxygen (marked as P4 in Figs. 5d and 5f). The aluminium oxide crumbs are an artefact that most likely occurred during the production of the battery.

To obtain more information about the different phases and to determine possible Li-contents, EDS point analyses were carried out at positions P1, P2 and P3 marked in Fig. 5 a. These were recorded with a landing energy of 3.5 keV and a beam current of 300 pA. The spectra are shown in Fig. 5 g. Two magnified sections are inserted as insets: the area of the Li peak and the area of the Al-Kα and Si-Kα peaks. As expected, the spectrum P1 (blue line) on the graphite particle shows a high carbon peak and traces of oxygen and aluminium, which can be attributed to the co-analysis of the Al/O-rich crumbs present on the surface. When comparing the spectra from positions P2 (red spectrum) and P3 (green spectrum), P3 has the highest oxygen peak and P2 has the highest Si peak. Both spectra contain traces of aluminium, which also can be attributed to the co-analysis of the Al/O-rich crumbs. The enlarged section of the Li peak area is particularly interesting. Here, the green spectrum differs significantly from the blue and red spectrum and shows a Li-Kα (52 eV) peak with a small shoulder at the Si-Kα (92 eV) edge. The red spectrum shows the peak of the Si-Kα (92 eV) transition and the blue spectrum shows a very small portion of the Al-Kα (72 eV) transition. This example demonstrates that even in the presence of Si and Al, Li can be clearly detected. Since the occurrence of the Li peak was combined with the highest oxygen signal, a high oxygen occurrence can be used as an initial indication of Li deposition in aged batteries.

4. Li QUANTIFICATION

When an image contains material contrast, the questions that automatically follow are: What is the chemical difference, can it be quantified, how reliable are the results? EDS analysis can provide initial answers. It enables also quantitative analysis into the trace constituent range ($0.01 \leq C \leq 0.1$) [20], but consistently upcoming questions are: How reliable are EDS studies for real life application under not ideal conditions, what are the influences of etc. sample preparation, storage and spectrum processing. The topic reliability becomes particularly important when some of the theoretically assumed basic conditions cannot be met. This also applies to the quantitative analysis of battery materials using EDS. The basic assumptions are a homogeneous sample composition and a flat sample surface. Neither of these conditions are met when analysing the anode, cathode or separator surfaces of battery foils. Although the surface is flat in the case of cross-sectional preparations, the composition is not homogeneous. Therefore, a systematic study was carried out on $Li(Ni_xMn_yCo_z)O_2$ cathode material.

In order to prove the reliability of quantitative EDS analysis on Li-ion batteries, alternative sample preparation methods were used and a round robin test was performed. The subject was the stochiometric composition of the Ni:Mn:Co content of the cathode active material within a commercially Li-ion battery (LG21700M50T), where Ni, Mn and Co share one position, consequently $x + y + z = 1$. Table 1 show the different settings: Without contact to air (glove box => shuttle => SEM vacuum, named **shuttle**) or prepared in air (named **air**). Top view on a piece of cathode foil (topographic surface) or cross-section obtained with the Ar-ion miller (named **Ar-ion**) or mechanical polishing (named **section**, flat surface). Additionally coated with gold (4 nm, named **Au**) or carbon (10 nm, named **C**). Spectrum processing was standard based for all previous examination conditions. The next setting is standard-less and, therefore, automatically normalising the findings to 100 %, neglecting the Li-content (named **normalised**).

Table 1. Stoichiometric Ni:Mn:Co ratio and Li-content.

	Mn	Co	Ni	Li (wt%)
shuttle	5.94 ± 0.04	11.68 ± 0.05	82.39 ± 0.06	6.0 ± 0.,5
air	5.54 ± 0.06	11.29 ± 0.07	83.17 ± 0.10	6.1 ± 0.8
Au	5.49 ± 0.04	11.32 ± 0.06	83.19 ± 0.08	10.6 ± 0.8
C	5.56 ± 0.06	11.43 ± 0.08	83.01 ± 0.12	10.4 ± 0.7
Ar-ion	4.91 ± 0.03	11.04 ± 0.08	84.05 ± 0.08	6.4 ± 0.6
section	5.01 ± 0.14	11.09 ± 0.13	83.89 ± 0.25	PS: 5.6 ± 0.3 AS: 14.2 ± 1.9
normalised	5.38 ± 0.06	11.16 ± 0.05	83.45 ± 0.09	6.0 ± 0.1
ICPOES	5.80 ± 0.02	10.60 ± 0.03	83.60 ± 0.03	6.0 ± 0.1

At least 5-point and area spectra were recorded for all settings. All performed examinations deliver a stoichiometric relationship close to Ni:Mn:Co ratio of 8-1-1. This proves the robustness of this analysis technique. Additionally results obtained with ICP-OES (last row in Table 1) agree nicely with the EDS results. Furthermore, other institutes (ZSW Ulm, KIT Karlsruhe) have carried out EDS examinations of the same sample and for the same purpose. In summary, the relative deviations between methods, institutions and preparation techniques was less than 10 % for Ni and Co and less than 15 % for Mn-content. This means that the stoichiometric composition, the Ni:Mn:Co ratio in lithium-ion batteries, can be reliably determined using EDS.

The next challenge is to determine the Li-content quantitatively. One of the possible approaches is the "composition by difference method". In this method, EDS images and quantitative backscattered electron imaging (qBEI) are combined. In this process, all non-Li elements are quantified using EDS. A calibration curve is then plotted for the expected grey values of the backscattered electron image. The Li-content is then determined as the difference between the quantitative backscattered electron image and the value of the calibration curve [21].

In the following, a new approach was pursued. The idea is to determine the Li-content indirectly as the missing element fraction of unnormalised EDS analysis "Li determination by difference". A condition has been set to exclude spectra containing artefacts. This can easily happen, if for example, the analysis also includes binder phase components, which then distort the correct determination of the battery active material. The samples examined were commercially available $LiNiMnCoO_2$ batteries (LG21700M50T and LG18650HG2). Solely those spectra were taken into account for the quantification, where the oxygen wt% of the EDS spectra is ±3 wt% of the expected weight percent for oxygen in the compound $Li(Ni_8Mn_1Co_1)O_2$. The mean values of the Li weight percent for the analytic conditions are shown in Table 1, last column (LG21700M50T): shuttle: 6.0 ± 0.5 wt%; air: 6.1 ± 0.8 wt%; Au coated: 10.6 ± 0.8 wt%; C coated: 10.4 ± 0.7 wt%, argon ion milling: 6.4 ± 0.6 wt%. Point and area spectra were acquired for all settings, providing consistent results. Mechanical polishing preparation alone yields 5.6 ± 0.3 wt% for the point spectra and 14.2 ± 1.9 wt% for the area spectra for the Li determination. On the one hand, this is probably due to the loss of Li during sample preparation => higher Li values for the area spectra and on the other hand by contamination during the acquisition of the point spectra underestimation of the Li-content. The results of the studies performed with the conditions shuttle, air and Ar-ion milling agree nicely with the expectation of 6.4 wt% for a 100 % lithiated cathode material after the first formation cycle, where the gold, carbon coating leads to a significant overestimation of the Li-content and the mechanical polished section cannot deliver reliable results [22]. A second battery (LG18650HG2) was also examined for verification. This was an unused lithiated cell and it provided a Li-content for the cathode 6.01 ± 0.94 wt% also in good agreement with an expected value of 6.4 wt% after the formation process.

5. CONCLUSION AND OUTLOOK

It is important for the analytical examination, as exemplified here for Li-ion battery materials, that artefacts such as radiation damage, contamination and charging are avoided as good as possible. Their influence should be controlled by checking the Duane-Hunt limit, comparing the spectrum with a theoretical spectrum and taking an image after the analysis with a good surface sensitive imaging technique to detect radiation damage and contamination if present. The use of an EDS detector specifically designed to detect low energy X-rays (Oxford Extreme) allows examination at low acceleration voltages and currents. This allows Li to be detected in metal as well as in compounds. This is possible with an energy resolution such that Li-Kα and Si-Lα can

be distinguished. This means that Li-phases in Li-ion batteries can be clearly assigned.Li-compounds can be determined, shown here with Li_2O. It was also demonstrated that EDS by difference can be used to quantitatively determine the Li-content in $LiNiMnCoO_2$ batteries. This gives hope that this idea can be applied to future problems.

6. ACKNOWLEDGMENTS

The authors gratefully acknowledge the German BMBF (FKZ:03XP0317A) and BMWK (FKZ:16BZF320C) for financial support and the ZSW, KIT, Volker Knoblauch, Tim Schubert, E. Delz, K. Kukla, C. Weisenberger, T. Waldmann, J. Haß, H.G. Schweiger, L. Billmann for scientific support.

7. REFERENCES

[1] Xiaobing L, Holland J, Burgess S, Bhadare S, Yamaguchi S, Birtwistle D, Statham P and Rowlands N 2013 *Microsc. Microanal.* **19** (Suppl. 2). 1136-1137
[2] Hovington P, Lagacé M, Principe E, Burgess S, Guerfi A, Demers H, Gauvin R and Zaghib K 2015 *Microsc. Microanal.* **21** (Suppl. 3) 2357-2358
[3] Hovington P, Timoshevskii V, Bessette S, Burgess S, Statham P, Demers H, Gauvin R and Zaghib K 2017 *Microsc. Microanal.* **23** (Suppl. 1) 2024-2025
[4] Hovington P, Timoshevskii V, Burgess S, Statham P, Demers H, Gauvin R and Zaghib K 2016 *Microsc. Microanal.* **22** (Suppl. 3) 84-85
[5] Bessette S, Hovington P, Demers H, Golozar M, Bouchard P, Gauvin R and Zaghib K 2019 *Microsc. Microanal.* **25** 866-873
[6] Reimer L 1993 *Image formation in low-voltage scanning electron microscopy*. Tutorial texts in optical engineering. vol. 12. [Bellingham, WA: SPIE Press]
[7] William Duane W and Hunt F L 1915 *Phys. Rev.* **6** 166-172
[8] Goldstein J, *et al.* 2003 *Scanning electron microscopy and X-ray microanalysis. 3rd edition*. [New York, NY: Springer]
[9] Goldstein J, *et al.* 2018 *Scanning electron microscopy and X-ray microanalysis. 4th edition*. [new York, NY: Springer]
[10] T. Kister 2013 *MSc thesis*. [Ulm, Germany: University of Ulm]
[11] Mitchell D R G 2015 *Micron* **73** 36-46
[12] Hugenschmidt M, Adrion K, Marx A, Müller E and Gerthsen D 2021 *Microsc. Microanal.* **27** (Suppl. 1) 2022-2024
[13] Meyer J C, *et al.* 2012 *Phys. Rev. Lett.* **108** 196102
[14] Kaiser U, *et al.* 2011 *Ultramicroscopy* **111** 1239-1246
[15] Egerton R F 2012 *Microsc. Res. Techn.* **75** 1550-1556
[16] Golla-Schindler U, Benner G, Orchowski A and Kaiser U 2014 *Microsc. Microanal.* **20** 715-722

[17] Reimer L 1998 *Scanning electron microscopy. 2nd edition*. [Berlin-Heidelberg, Germany: Springer Verlag]
[18] Drouin D, Couture A R, Joly D, Tastet X, Aimez V and Gauvin R 2007 *Scanning* **29** 92-101
[19] Eggert F 2020 *Microsc. Today* **28** (2) 34-39
[20] Newbury D and Ritchie N 2019 *Microsc. Microanal.* **25** 1075-1105
[21] Österreicher J, Simson C, Großalber A, Frank S W and Gneiger S 2021 *Scripta Materialia* **194** 113664
[22] Golla-Schindler U, Barbosa Sa E, Weisenberger C, Knoblauch V and Schneider G 2023 *Microsc. Microanal.* **29** (Suppl. 1) 117-118